Charge-Neutralized Colloids for Waterborne High-Energy Dielectrics

Junjin Che, Cécile Zakri, Isabelle Ly, Wilfrid Neri, Eric Laurichesse, Jean-Paul Chapel, Philippe Poulin, Jinkai Yuan*

Centre de Recherche Paul Pascal, CNRS, Université de Bordeaux, UMR 5031, 33600 Pessac, France
E-mail: jinkai.yuan@crpp.cnrs.fr (J.Y.)

Abstract

Colloids are attractive building blocks for the assembly of organized functional materials. However, their stabilizing surface charges limit the high voltage tolerance and the capacitive energy storage of resultant solid films, which has long remained challenging for dielectric applications of colloids. Here, we propose a strategy of electrostatically complexing colloids with oppositely charged polyelectrolytes to neutralize their surface charges and achieve waterborne high-energy dielectrics. Polyvinylidene fluoride latex, a reference dielectric polymer, interacts electrostatically with a biosourced polycation, chitosan, to generate hybrid particles with tunable surface charge properties. The presence of chitosan prevents the coalescence of the latex particles, yet drives their assembly to form closely packed heterogeneous films. At the isoelectric point where the dispersion exhibits a *zeta* potential close to 0, the resulting nanocomposites demonstrate the highest Weibull breakdown strength (630 MV/m) and recoverable energy density (10.1 J/cm^3), which are respectively 279% and 421% higher than the coalesced counterpart. The validated principle has been successfully extended to other colloidal systems, such as polystyrene latex and aqueous bentonite suspension, highlighting the versatility of the proposed approach to develop waterborne high-energy dielectric materials.

Keywords: Colloids, Polyelectrolytes, Electrostatic complexation, PVDF latex, Chitosan, Dielectrics, Energy storage

1. **Introduction**

Dielectric materials are capable of storing energy in the form of electric displacement upon application of an electric field. This energy storage mechanism endows them an intrinsic fast energy uptake and delivery with times ranging from nanoseconds to milliseconds.(*1*) The electrostatic capacitors based on dielectric materials are increasingly pervasive in modern electronics and pulsed power systems.(*2-5*) Nevertheless, capacitors generally have lower energy densities compared with other electrochemical energy storage systems such as batteries.(*6*) Today, many of the advanced electronic and electrical systems require high integration, compactness, and miniaturization, leading to the rapid development of new dielectrics that have high energy density and high efficiency.(*7-10*)

The energy built up in dielectric materials is determined by the applied electric field E and the consequent dielectric polarization P. The maximum stored energy density U_s is expressed as $\int_0^{P_m} E dP$, where P_m is the maximum polarization.(*11*) Yet only a portion of the stored energy can be effectively discharged due to the existence of hysteresis losses, leading to a remnant polarization, P_r. The discharged energy density U_d can then be calculated as $\int_{P_r}^{P_m} E dP$ (Supplementary Fig.1).(*12*) The energy storage efficiency is defined as U_d/U_s. Thus, a combination of large polarization variation (P_m-P_r) and high breakdown strength E_b is highly desired to achieve a high U_d.(*13*)

Conventional dielectric materials are ceramics with large spontaneous polarization and excellent thermal stability.(*14*) Yet they suffer from low breakdown strength and challenging processing conditions.(*15*) As alternatives, polymers have facile processability, high breakdown strength, and low energy losses.(*10, 16, 17*) However, their low permittivity ($k<10$) poses a critical

challenge for the technological implementation in miniaturized devices. Due to the inverse correlation between the polarization and breakdown strength ($E_b = k^{-0.65}$), (18) the achieved U_d to date is still limited (<5 J/cm^3) for capacitors based on ceramics or polymers alone.(2) Some strategies have emerged to further enhance U_d via developing polymer nanocomposites with disparate components/phases, such as designing novel morphology of hybrid fillers,(19-21) modulating macromolecular organizations,($16, 22$-24) creating multilayered structures,($11, 25$-30) and establishing dielectric anisotropy.(31-34)

Being different, we target high-energy dielectric materials by colloidal engineering. Colloids have been used as building blocks to construct diverse functional materials with emergent physical properties(35), such as proton conductive membranes(36), plasmonic nanostructures(37), organic photovoltaic devices($38, 39$), and field-effect transistors(40). However, it has long remained challenging to create dielectric films using colloidal building blocks. Generally, water-based colloids are electrostatically stabilized by surface charges. The high density of charges on the particle surface create conductive paths. These highly conductive domains induce significant leakage and dramatically reduce the breakdown strength of the solidified material. To the best of our knowledge, high-energy colloidal films are lacking until now. Here, we propose to electrostatically complex colloids with oppositely charged polyelectrolytes to neutralize their surface charges and develop waterborne high-energy dielectrics.

2. Results and Discussion

We start from water-based polyvinylidene fluoride (PVDF) latex with low cost, environmental friendliness, and particularly the known high permittivity. The PVDF latex dispersion can remain as individual particles for an appreciable time (**Figure 1a**). Such

electrostatic stabilization arises from the dissociation of the carboxylic groups on the latex nanoparticles. Protonated chitosan (NH_3^+), a biosourced water-soluble polymer, is chosen as a cationic polyelectrolyte to electrostatically interact with latex nanoparticles and to finely control the charge neutralization of generated hybrid particles. The PVDF@Chitosan dispersions display distinct scenarios depending on the fraction of chitosan $f_{Chitosan}$ (**Figure 1a**).

At low $f_{Chitosan}$ up to 0.3%, stable PVDF latex particles are partially decorated with chitosan chains, generating individual hybrid particles with a net negative charge (*zeta* potential<-43 mV, **Figure 1b, c**, Supplementary Table 1). By increasing the fraction up to 0.6%, the negative surface charges carried by the PVDF latex particles are progressively compensated by the cationic groups (NH_3^+) present on the chitosan chains and by the decreased pH. But the amplitude of the *zeta* potential still remains above 30 mV, a critical value, above which a colloidal suspension is considered to be electrostatically stabilized.(*41*) However, the size of the complexes increases by an order of magnitude (Supplementary Table 1), suggesting that bridging or complexation between the latex particles by the chitosan chains is the dominant mechanism involved at this stage. Such bridging is a consequence of the adsorption of the segments of individual chitosan chain onto the surfaces of more than one PVDF particle (**Figure 1b**). In the vicinity of 0.8%, the hybrid particles become significantly less charged, and are then subject to increasing hydrophobic interactions. The dispersion becomes unstable with the formation of loose and jammed assemblies as a result of the Brownian collisions of hybrid particles. Near this point, bridging may still be operational, but the mass ratio corresponds quite closely to the dosage of chitosan required to neutralize the surface charge of the PVDF particles. Such charge neutralization is experimentally revealed by the reduction of the measured electrophoretic mobility of the particles to nearly zero (the isoelectric

point), the pH down to 7 (Supplementary Table 1), and the increase of colloid size to the largest

value (~6.5 μm, **Figure 1c**). At higher fractions beyond 1%, a neat charge reversal occurs due to

the macromolecular nature of the chitosan chains, yielding more charged and stable cationic hybrid

particles with much smaller sizes (**Figure 1c**). The *zeta* potential then becomes more and more

positive with values above +30mV, promoting a very stable dispersion. At this stage, steric and

electrosteric stabilization start to take place. (*41*)
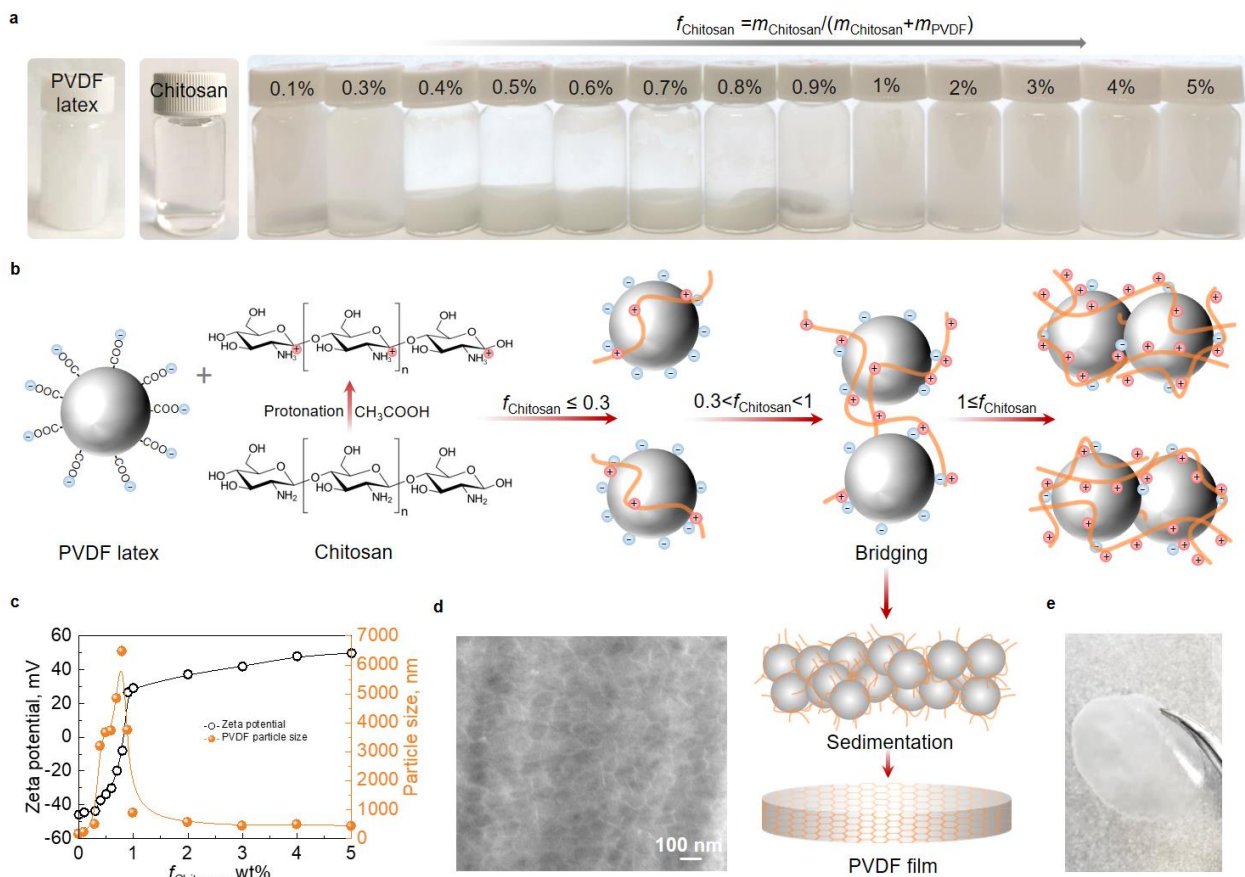
Figure 1. PVDF@Chitosan complexes and waterborne dielectric films. a) Photographs of PVDF latex dispersion (0.72 wt%), aqueous chitosan solution (0.66 wt%), and their mixtures at different mass ratios. b) Schematic illustrations of the electrostatic interactions between negatively charged PVDF particles and cationic chitosan chains at different stages of mass ratios. By increasing the $f_{Chitosan}$, the pH of dispersions decreases, the latex particles and chitosan macromolecules become less and more charged respectively. c), *Zeta* potential of the different dispersions as well as the size of the PVDF@Chitosan complexes as a function of the mass ratio. d) TEM image, e) photograph of a free-standing waterborne PVDF@Chitosan dielectric film with a $f_{Chitosan}$ of 0.8%.

The complexation of PVDF and chitosan screens their Coulombic attraction with respective counterions. In particular, at the isoelectric point (0.8 %), all charged latex particles and chitosan chains presumably engage in the formation of complexes through ion-pairing, promoting a complete liquid-solid phase separation with the release of all counterions into the supernatant phase. This mechanism is highly analogous to the widespread associative process of oppositely charged polyelectrolytes in aqueous solutions.(*42*) Intriguingly, the charge-neutralized PVDF@Chitosan complexes are film forming under infrared light, yielding freestanding waterborne films, showing a segregated nanostructure with a clear boundary between the PVDF nanoparticles (**Figure 1d)**. Indeed, the chitosan chains wrapped around the PVDF nanoparticles prevent their coalescence. The resulting hybrid and segregated nanostructure is extremely stable and can be maintained even after hot pressing at 110°C. Actually, chitosan has excellent film-forming properties. Not only does it drive the assembly of PVDF latex particles, but it also fills the voids or cracks that usually form when water evaporates from the colloidal dispersion. **Figure 1e** shows a photograph of a freestanding PVDF@Chitosan dielectric film. The patterned latex films are typically ~10 µm thick and are highly uniform, flexible, and crack-free.

To confirm the potential dielectric applications of PVDF@Chitosan complex films, we examine their structural, mechanical and dielectric properties and compare them with coalesced PVDF latex films. **Figure 2a** schematizes the formation of pure PVDF latex films. As the water evaporates, the uniformly and stably dispersed bare PVDF particles come into contact with each other. When PVDF latex particles have reached their maximum packing, compression and coalescence of the particles begin towards the formation of a continuous film. Additional thermal annealing is used to remove defects, remaining voids or cracks after the film has solidified. The

cross-sectional scanning electron microscope (SEM) images confirm the coalescence of PVDF nanoparticles into a continuous single phase (**Figure 2b, c**). On the other hand, the PVDF@Chitosan system, due to the bridging and compensation of positive and negative charges, undergoes a liquid-solid phase separation eventually leading to gravity sedimentation over time (**Figure 2d**). After removing the supernatant, the sediment is readily cast into thin films. Due to the existence of chitosan coating on the surface of PVDF nanoparticles, they are not able to fully contact each other. The presence of chitosan chains ultimately prevents the complete coalescence of PVDF nanoparticles yet promotes the self-assembly of PVDF nanoparticles into a closely packed heterogeneous film (**Figure 2e, f**).

The tensile properties of waterborne PVDF latex films and PVDF@Chitosan films have been characterized and compared with typical solvent-processed PVDF polymers. Latex films display mechanical properties distinct from conventional PVDF films (**Figure 2g**). They are not as stiff as the latter, exhibiting lower Young's moduli. However, latex films can withstand a large plastic deformation (~820%) before break, which is 64 times higher than that of typical PVDF film. Such mechanical behaviors are highly akin to thermoplastic elastomers.(*43*) Furthermore, as compared to the coalesced PVDF latex film, Young's modulus of PVDF@Chitosan film decreases by 50%, yet the elongation at break and ultimate tensile strength decline only by 7% and 10% respectively. In essence, the non-coalesced PVDF@Chitosan films retain the mechanical strength of latex particles, and are still mechanically sound for further applications.
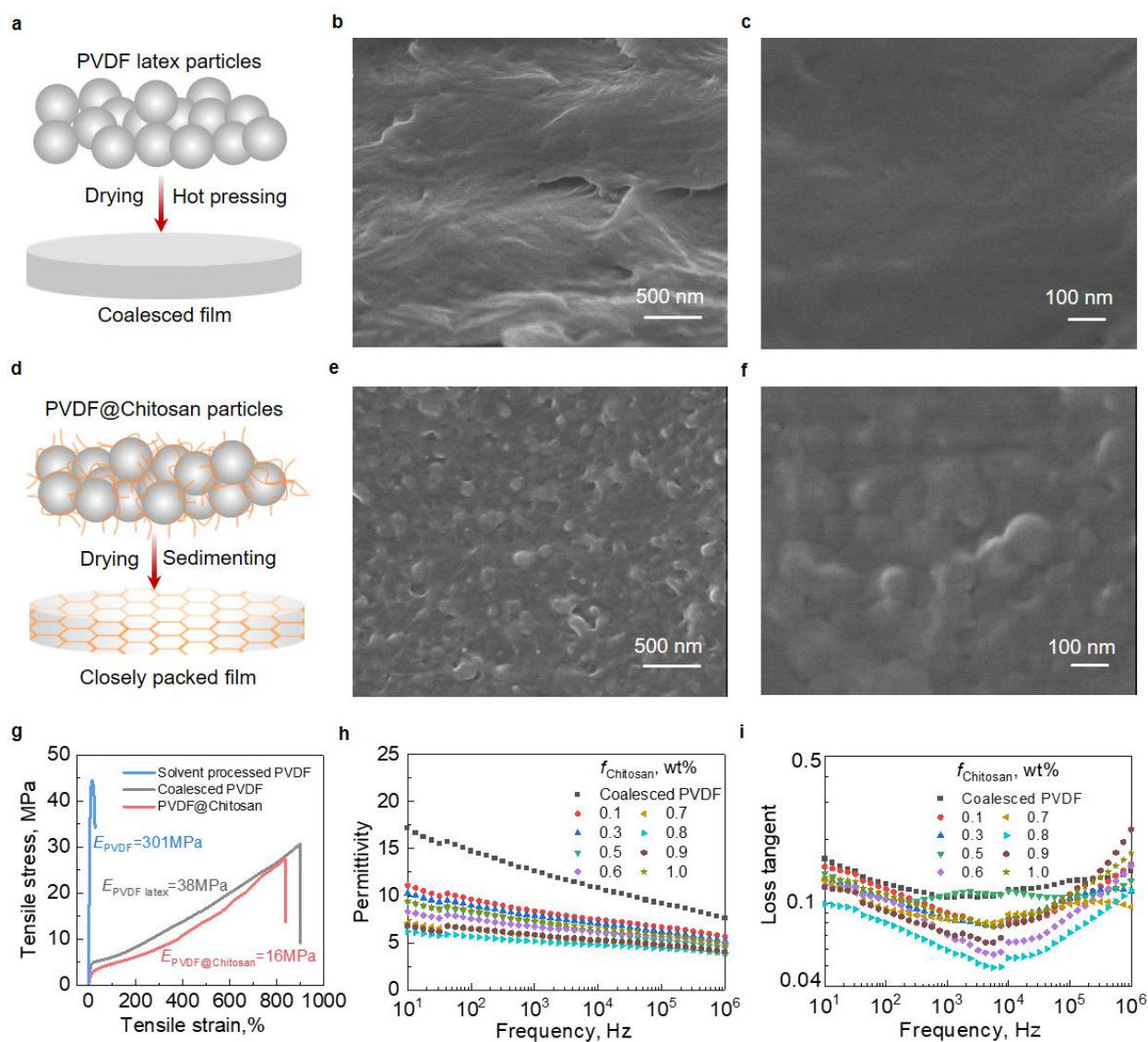
Figure 2. Morphology, mechanical and dielectric properties. a) Schematic illustration of the inner structure of the coalesced latex films. b,c) SEM images under different magnifications for a cross-sectional PVDF latex film directly cast from the latex dispersion, followed by hot-pressing at 110°C. d) Schematics of the heterogeneous structure of PVDF@Chitosan film. e,f) The cross-sectional SEM images of PVDF@Chitosan film, which is derived from a mixture dispersion with a $f_{Chitosan}$ of 0.8%, followed by incubation at 60°C and hot pressing at 110°C. g) The tensile stress versus tensile strain curves for typical PVDF processed in N,N-dimethylformamide, waterborne PVDF latex film and PVDF@Chitosan film at $f_{Chitosan}$ of 0.8%. Young's modulus, E, of each film is indicated in the figure. h) Frequency dependence of permittivity for coalesced PVDF latex and PVDF@Chitosan films. i) Loss tangent of coalesced PVDF latex and PVDF@Chitosan films as a function of frequency.

We further performed dielectric characterizations of PVDF latex samples to explore their potential for capacitive energy storage. **Figure 2h** shows the permittivity of PVDF latex films as a function of frequency and the fraction of chitosan used to neutralize charges of PVDF nanoparticles. The coalesced PVDF latex film displays a drop of apparent permittivity at low frequency. This arises from the polarization of the electrodes as a result of the formation of the electric double layer, in which the charges on the electrodes are balanced by the adsorption of mobile charges present in the latex film. Due to the existence of such mobile charges, the apparent permittivity is higher than solvent- or melt-processed PVDF films (k~10) (*44, 45*), and accompanied by a relatively large dielectric loss (tanδ>0.1, **Figure 2i**). The same mechanism is illustrated in ion-containing polyvinyl alcohol (PVA) films (Supplementary Fig. 2). On the other hand, the permittivity of PVDF@Chitosan films decreases continuously and becomes less frequency-dependent as the level of charge neutralization of hybrid particles increases (**Figure 1c**, **Figure 2h**). A similar downward trend is also found for loss tangent. At the critical isoelectric point (0.8%), the material demonstrates the lowest loss (0.05@10 kHz), and exhibits a permittivity of 6. Beyond the isoelectric point, the additional chitosan chains reverse the neat charge and promote an increasing charge density on the formed complexes. This in turn gives rise again to large losses and permittivity, as evidenced by the dielectric spectroscopy of PVDF@Chitosan films with elevated $f_{Chitosan}$ ranging from 1 wt% to 5 wt% (Figure S3).

Generally, as compared to solvent- or melt-processed materials, waterborne polymer films tend to contain relatively more charged species and suffer from lower breakdown strength. However, the improved insulating properties of PVDF@Chitosan films at $f_{Chitosan}$ of 0.8% hold great promise to withstand a high voltage. To confirm this key feature for capacitive energy storage,

we recorded the voltages applied incrementally until the dielectric breakdown. The E_b and shape

factor β are calculated by a linear fit using the Weibull failure statistics (**Figure 3a**, Table S2). E_b

of coalesced PVDF latex film is found to be 226 MV/m, which is much lower than those (from

350 MV/m to 400 MV/m) achieved in typical PVDF films via conventional solution casting or

melt-extrusion.(*44, 46, 47*) The reason is the presence of free charge carriers in the waterborne

coalesced PVDF latex film. The mobile charges on the particle surfaces migrate easily under a

high electric field. They induce Joule heating and make the material susceptible to breakdown.

Such effect of mobile ions on E_b has been also verified in solid ion-containing PVA/CH$_3$COONa

films (Figure S4). However, the introduction of a trace amount of chitosan greatly improves the

breakdown strength of PVDF latex films. The E_b of PVDF@Chitosan film continuously increases

with chitosan content and reaches a maximum value of 630 MV/m at the isoelectric point (0.8

wt%), representing an improvement of 179% (**Figure 3b**). This behavior can be understood by

considering the charge compensation process by ion-pairing and the morphology of resulting

PVDF@Chitosan films. As they approach isoelectric point, the negatively charged PVDF

nanoparticles are progressively neutralized and linked together via chain bridging and/or

hydrophobic interactions. The resultant large assemblies sediment, releasing counterions from the

solid phase to the aqueous liquid phase. In this regard, a lower density of charges remain on the

surface of PVDF@Chitosan hybrid particles, with which the built film has a higher breakdown

strength. In addition, PVDF nanoparticles are wrapped by chitosan chains, which prevent their

coalescence and promote their self-assembly into a very compact but heterogeneous film. Such

structure is highly favorable to eliminate leakage currents with barriers or traps between

polarizable PVDF particles. (*48*) The formed convoluted paths staunch the initiation

and propagation of electrical treeing, leading to high E_b.(*34*) The neutral charge state of PVDF@Chitosan complexes, together with the heterogeneous nanostructures, contributes to the conspicuous improvement of the breakdown strength. Beyond the isoelectric point, the breakdown strength declines rapidly with the addition of more chitosan chains (**Figure 3b**, Figure S5). At this stage, the heterogeneous nanostructure can always remain, but the excessive chitosan promotes an increasing density of dissociated charges located at the particle boundaries and makes the barrier conductive. The formed conductive paths induce leakage and reduce the breakdown strength.

Thanks to the adequately enhanced E_b, a waterborne high-energy dielectric can be clearly envisioned. We characterized the polarization and energy storage density of PVDF@Chitosan films at high electric fields. The polarization-electric field (*P-E*) hysteresis loops of each film were first measured under an electric field (200 MV/m), which is close to the E_b of bare PVDF latex film. With increasing $f_{Chitosan}$, the maximum electric displacement P_m decreases yet the hysteresis loop becomes thinner (reduced P_r), both reaching the limit at 0.8 wt% (**Figure 3c**). This indicates that the neutralization of PVDF nanoparticles partially loses the polarization capacity related to ion activities in the system but gains a larger portion of the discharged energy. The polarization of fully charge-neutralized PVDF based film is evaluated at fields up to E_b (**Figure 3d**). P_m-P_r increases with the electric field and reaches 40 mC/m^2 at 630 MV/m. The discharged energy density U_d and efficiency η are then calculated from the *P-E* loops of each film (**Figure 3e**). Combining the excellent P_m-P_r and highest E_b, the PVDF@Chitosan film at $f_{Chitosan}$ of 0.8% achieves the highest U_d of 10.1 J/cm^3, which is 4.2 times higher than bare latex film (U_d=2.4 J/cm^3), and more than twice of typical PVDF materials.(*46*) The high U_d should be ascribed to the low loss (small P_r) of the charge-neutralized PVDF@Chitosan assemblies and the greatly improved E_b

by the surface charge neutralization and the formed heterogeneous nanostructure. In addition, the η is higher than its counterparts at each field, and maintains high values of ~72% as the electric fields approach E_b. The high efficiency is also associated with low dielectric loss and suppressed leakage current in the charge-neutralized system. Above the isoelectric point, excessive chitosan fractions (from 0.9 wt% to 5 wt%), however, lead to a degraded energy storage performance due to decreased E_b and increased conduction losses, both of which lead to a striking decrease in efficiency (Figure S6).

Figure 3f compares the U_d and η values of our charge-neutralized PVDF film with those of recently reported high-energy-density polymer-based dielectrics, including all-organic polymers,(*22, 49-59*) and inorganic/organic nanocomposites.(*3, 60*) Indeed, our charge-neutralized PVDF film exhibits concurrently high U_d and η. In addition, most polymer dielectrics are either melt-extruded at high temperatures or processed in hazardous organic solvents. Their manufacturing process is, therefore, energy-consuming and environmentally problematic. Our strategy based on soft-chemistry processes holds great potential for environmentally friendly high-performance capacitors.
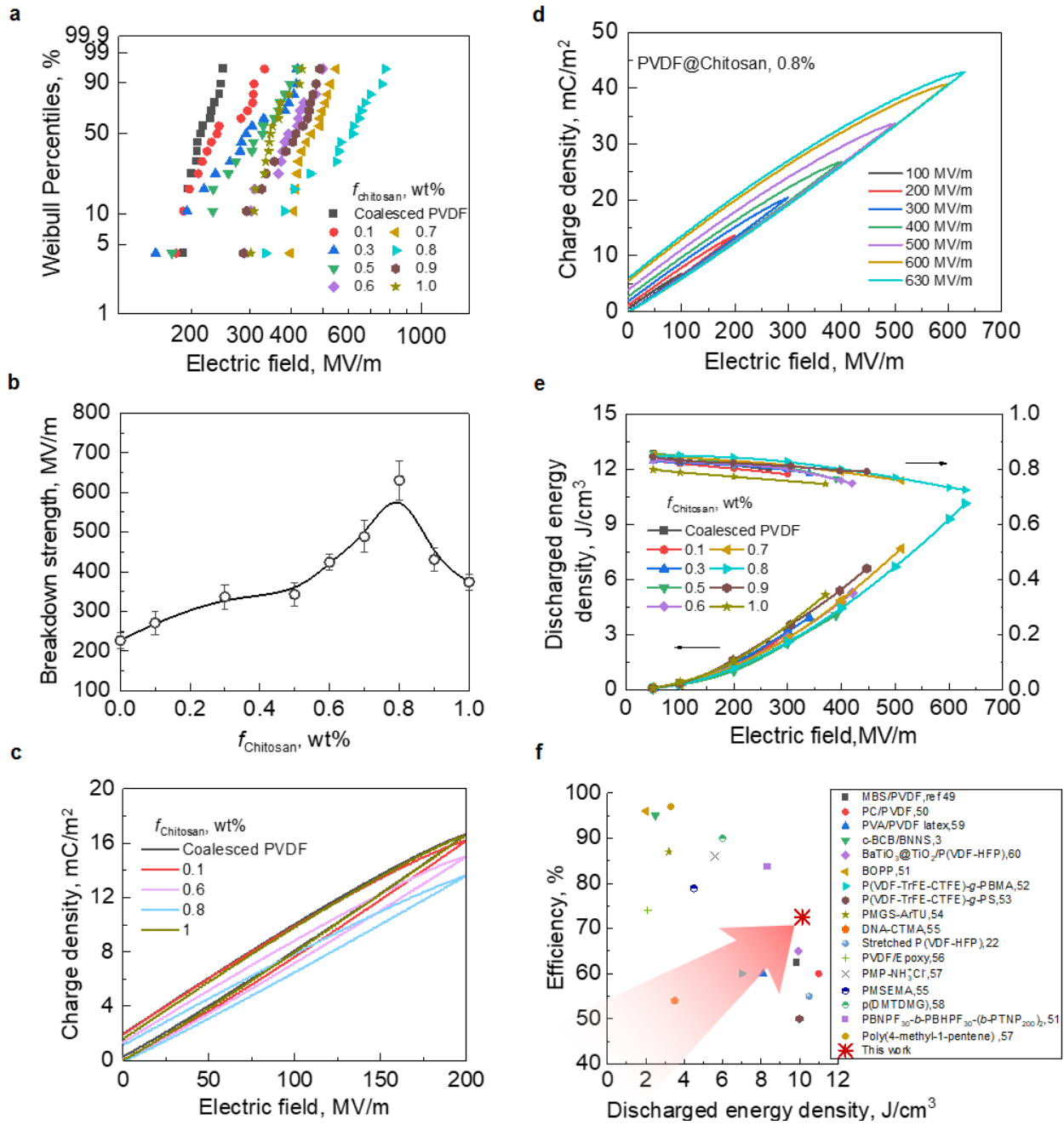
Figure 3. Breakdown strength and energy storage performances. a) Failure probability of dielectric breakdown deduced from Weibull distribution. The E_b and shape factor β are listed in Table S2. b) E_b for coalesced PVDF latex and PVDF@Chitosan films at various chitosan fractions. c) $P-E$ loops of coalesced PVDF latex and PVDF@Chitosan films at 200 MV/m. d) $P-E$ loops of PVDF@Chitosan film with f_{Chitosan} of 0.8% at different electric fields. e) Discharged energy density and charge/discharge efficiency as a function of electric field for coalesced PVDF latex and PVDF@Chitosan films. f) The comparison of discharged energy density and charge/discharge efficiency for PVDF@Chitosan film with f_{Chitosan} of 0.8% and state-of-the-art dielectric polymers.

13

To evaluate power density and reliability, fast charge/discharge cycles were performed on the PVDF@Chitosan film ($f_{Chitosan}$=0.8%) and a commercial biaxial oriented polypropylene (BOPP) film using a typical high-speed capacitor circuit.(*59*) The two samples are initially charged at 200 MV/m and then discharged across a 10 kΩ load resistor in series with the sample capacitor (**Figure 4a**). The discharged energy density is plotted as a function of time, where the discharge time is defined as the time required to achieve 95% of the final discharged energy. The PVDF@Chitosan film liberates a stored energy of 1.148 J/cm^3 at a rate of 1.248 µs, while the BOPP releases a stored energy of 0.299 J/cm^3 at a rate of 1.168 µs (**Figure 4b**). Accordingly, the PVDF@Chitosan film exhibits a higher power density (0.92 MW/cm^3) as compared to 0.26 MW/cm^3 of BOPP. Moreover, the energy density of the PVDF@Chitosan films remains constant without degradation over continuous 7000 cycles of charge/discharge (**Figure 4c**). In addition, the leakage current is another essential characteristic for practical applications. We performed the *P-E* loop test at a constant electric field and recorded the leakage current (**Figure 4d**). The leakage current density is suppressed by one order of magnitude at charge neutralization, from 2×10^{-5} A/cm^2 ($f_{Chitosan}$ =0) to 10^{-6} A/cm^2 ($f_{Chitosan}$=0.8%) at the electric field of 100 MV/m, reaching the lowest level (highest resistivity) which can rival most of the recently reported high-energy dielectric materials.(*2, 12, 13, 29*) The great improvement of the resistivity should be ascribed to the suppression of mobile charges by the charge neutralization at the critical mass ratio (0.8 wt%) in the PVDF@Chitosan hybrid system. Combining all these merits, the charge-neutralized PVDF latex film shows great potential for practical dielectric energy storage applications.
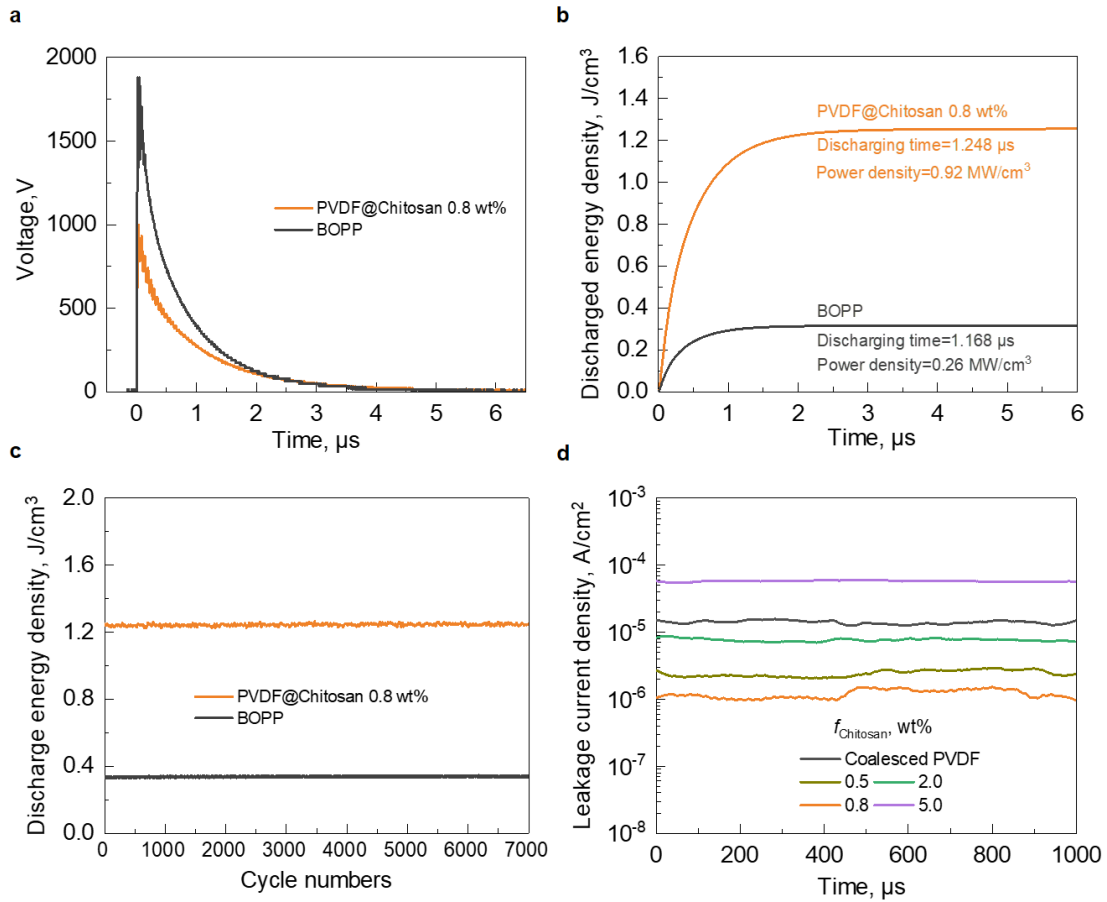
Figure 4. Charge/discharge performances. a) The voltage, and b) discharged energy density as a function of time during a charge/discharge cycle. c) Cyclic charge/discharge performances of the PVDF@Chitosan film at $f_{Chitosan}$ of 0.8% and the BOPP film in response to a charging electric field of 200 MV/m. d) The leakage currents at a constant electric field of 100 MV/m for PVDF@Chitosan at different $f_{Chitosan}$.

Furthermore, we experimentally extended the concept validated in the PVDF latex system to polystyrene (PS) latex and aqueous bentonite suspensions (Supplementary Text), which are stabilized by negative charges and represent organic and inorganic colloids respectively. Two waterborne colloidal films, PS@Chitosan and Bentonite@Chitosan, are prepared by charge neutralization at chitosan fractions of 1.1 wt% and 10 wt% respectively. At the isoelectric point, the PS@Chitosan film exhibits an E_b of 320 MV/m and an energy density of 1.4 J/cm^3, which show improvements of 28% and 180% over the pure PS latex films, respectively (Figure S10). In

addition, the resulting Bentonite@Chitosan/PVA film show the maximum energy density of 5.6 J/cm^3 at 388 MV/m (Figure S15). In contrast, the chitosan-free Bentonite/PVA composite loses the capability of energy storage beyond an electric field of 160 MV/m due to the presence of massive mobile charges in the film.

3. Conclusion

We proposed a charge neutralization strategy to substantially enhance the breakdown field and reduce the hysteretic losses of waterborne dielectrics created with colloidal building blocks. A high energy density of 10.1 J/cm^3 and an efficiency of 72% were achieved at 630 MV/m in charge-neutralized PVDF latex film. The finding is generic and validated in other dielectric materials manufactured from dispersions of polystyrene latex and aqueous bentonite suspension, opening thereby a widely applicable paradigm for the realization of waterborne high-energy dielectric materials.

References

1. Li, H. *et al.* Enabling High-Energy-Density High-Efficiency Ferroelectric Polymer Nanocomposites with Rationally Designed Nanofillers. *Adv. Funct. Mater.* **31**, 2006739 (2021).

2. Pan, H. *et al.*, Ultrahigh-energy density lead-free dielectric films via polymorphic nanodomain design. *Science* **365**, 578-582 (2019).

3. Li, Q. *et al.* Flexible high-temperature dielectric materials from polymer nanocomposites. *Nature* **523**, 576-579 (2015).

4. Dang, Z. *et al.* Fundamentals, processes and applications of high-permittivity polymer matrix composites. *Prog. Mater. Sci.* **57**, 660-723 (2012).

5. Chu, B. *et al.*, A dielectric polymer with high electric energy density and fast discharge speed. *Science* **313**, 334-336 (2006).

6. Simon, P. & Gogotsi, Y. Materials for electrochemical capacitors. *Nat. Mater.* **7**, 845-854 (2008).

7. Palneedi, H. *et al.* High-Performance Dielectric Ceramic Films for Energy Storage Capacitors: Progress and Outlook. *Adv. Funct. Mater.* **28**, 1803665 (2018).

8. Dang, Z. *et al.* Flexible Nanodielectric Materials with High Permittivity for Power Energy Storage. *Adv. Mater.* **25**, 6334-6365 (2013).

9. Xu, B., Íñiguez, J. & Bellaiche, L. Designing lead-free antiferroelectrics for energy storage. *Nat. Commun.* **8**, 1-8 (2017).

10. Tan, D. Q. Review of Polymer-Based Nanodielectric Exploration and Film Scale-Up for Advanced Capacitors. *Adv. Funct. Mater.* **30**, 1808567 (2020).

11. Bai, H., Zhu, K., Wang, Z., Shen, B. & Zhai, J. 2D Fillers Highly Boost the Discharge Energy Density of Polymer-Based Nanocomposites with Trilayered Architecture. *Adv. Funct. Mater.* **31**, 2102646 (2021).

12. Kim, J. *et al.* Ultrahigh capacitive energy density in ion-bombarded relaxor ferroelectric films. *Science* **369**, 81-84 (2020).

13. Yang, B. *et al.* High-entropy enhanced capacitive energy storage. *Nat. Mater*, 1-7 (2022).

14. Wang, G. *et al.* Electroceramics for High-Energy-Density Capacitors: Current Status and Future Perspectives. *Chem. Rev.* **121**, 6124-6172 (2021).

15. Yao, Z. *et al.* Homogeneous/Inhomogeneous-Structured Dielectrics and their Energy-Storage Performances. *Adv. Mater.* **29**, 1601727 (2017).

16. Zhang, Q. *et al.* High-temperature polymers with record-high breakdown strength enabled by rationally designed chain-packing behavior in blends. *Matter* **4**, 2448-2459 (2021).

17. Wu, X., Chen, X., Zhang, Q. M. & Tan, D. Q. Advanced dielectric polymers for energy storage. *Energy Stor. Mater.* **44**, 29-47 (2022).

18. McPherson, J. W., Kim, J., Shanware, A., Mogul, H. & Rodriguez, J. Trends in the ultimate breakdown strength of high dielectric-constant materials. *IEEE Trans. Electron Devices.* **50**, 1771-1778 (2003).

19. Zhang, X. *et al.* Ultrahigh Energy Density of Polymer Nanocomposites Containing
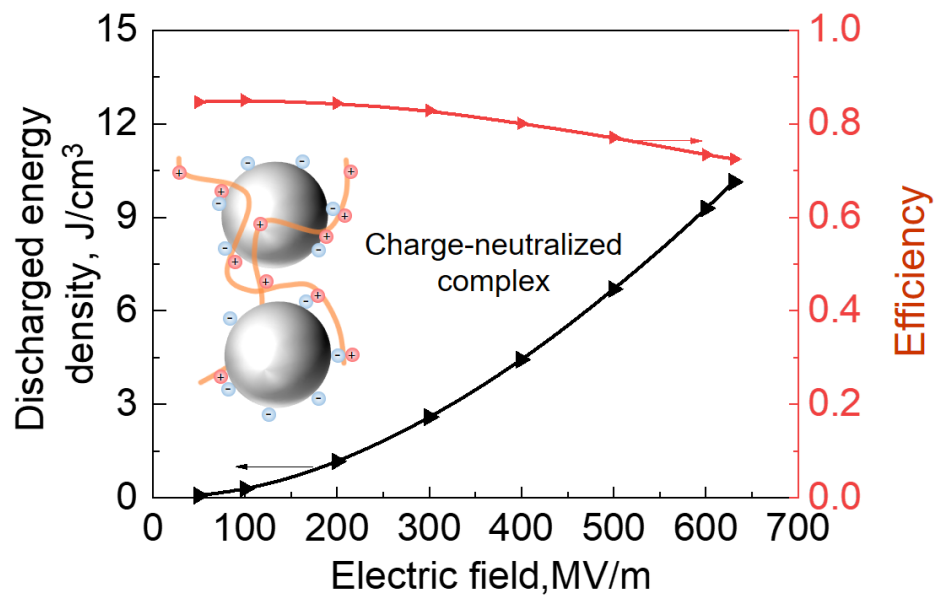
BaTiO3@TiO2 Nanofibers by Atomic-Scale Interface Engineering. *Adv. Mater.* **27**, 819-824 (2015).

20. Huang, X. & Jiang, P. Core–shell structured high-k polymer nanocomposites for energy storage and dielectric applications. *Adv. Mater.* **27**, 546-554 (2015).

21. Ren, L. *et al.* High-Temperature High-Energy-Density Dielectric Polymer Nanocomposites Utilizing Inorganic Core-Shell Nanostructured Nanofillers. *Adv. Energy Mater.* **11**, 2101297 (2021).

22. Guan, F., Pan, J., Wang, J., Wang, Q. & Zhu, L. Crystal Orientation Effect on Electric Energy Storage in Poly(vinylidene fluoride-co-hexafluoropropylen) Copolymers. *Macromolecules* **43**, 384-392 (2010).

23. Meng, N. *et al.* Ultrahigh beta-phase content poly(vinylidene fluoride) with relaxor-like ferroelectricity for high energy density capacitors. *Nat. Commun.* **10**, 1-9 (2019).

24. Zhang, T. *et al.* A highly scalable dielectric metamaterial with superior capacitor performance over a broad temperature. *Sci. Adv.* **6**, eaax6622 (2020).

25. Jiang, J. *et al.* Synergy of micro-/mesoscopic interfaces in multilayered polymer nanocomposites induces ultrahigh energy density for capacitive energy storage. *Nano Energy* **62**, 220-229 (2019).

26. Baer, E. & Zhu, L. 50th Anniversary Perspective: Dielectric Phenomena in Polymers and Multilayered Dielectric Films. *Macromolecules* **50**, 2239-2256 (2017).

27. Jiang, Y. *et al.* Ultrahigh Breakdown Strength and Improved Energy Density of Polymer Nanocomposites with Gradient Distribution of Ceramic Nanoparticles. *Adv. Funct. Mater.* **30**, 1906112 (2020).

28. Sun, L. *et al.* Asymmetric Trilayer All-Polymer Dielectric Composites with Simultaneous High Efficiency and High Energy Density: A Novel Design Targeting for Advanced Energy Storage Capacitors. *Adv. Funct. Mater.* **31**, 2100280 (2021).

29. Wang, T. *et al.* 2-2 Type PVDF-Based Composites Interlayered by Epitaxial (111)-Oriented BTO Films for High Energy Storage Density. *Adv. Funct. Mater.* **32**, 2108496 (2022).

30. Goodman, S. M., Che, J., Neri, W., Yuan, J. & Dichiara, A. B. Water-processable cellulosic nanocomposites as green dielectric films for high-energy storage. *Energy Stor. Mater* **48**, 497-506 (2022).

31. V. Tomer, C. A. Randall, G. Polizos, J. Kostelnick, E. Manias, High- and low-field dielectric characteristics of dielectrophoretically aligned ceramic/polymer nanocomposites. *J. Appl. Phys.* **103**, 034115 (2008).

32. Tang, H., Lin, Y. & Sodano, H. A. Enhanced energy storage in nanocomposite capacitors through aligned PZT nanowires by uniaxial strain assembly. *Adv. Energy Mater.* **2**, 469-476 (2012).

33. Jiang, Y. *et al.* Ultrahigh Energy Density in Continuously Gradient-Structured All-Organic Dielectric Polymer Films. *Adv. Funct. Mater.* **32**, 2200848 (2022).

34. Shen, Z. *et al.* High-Throughput Phase-Field Design of High-Energy-Density Polymer Nanocomposites. *Adv. Mater.* **30**, 1704380 (2018).

35. Renna, L. A., Boyle, C. J., Gehan, T. S., & Venkataraman, D. Polymer nanoparticle assemblies: a versatile route to functional mesostructures. *Macromolecules* **48**, 6353-6368 (2015).

36. Gao, J., Yang, Y., Lee, D., Holdcroft, S. & Frisken, B. J. Self-assembly of latex particles into proton-conductive membranes. *Macromolecules* **39**, 8060-8066 (2006).

37. Patoka, P. & Giersig, M. Self-assembly of latex particles for the creation of nanostructures with tunable plasmonic properties. *J. Mater. Chem.* **21**, 16783 (2011).

38. Gehan, T. S. *et al.*, Multiscale Active Layer Morphologies for Organic Photovoltaics Through Self-Assembly of Nanospheres. *Nano Lett* **14**, 5238-5243 (2014).

39. Kietzke, T. *et al.*, Novel approaches to polymer blends based on polymer nanoparticles. *Nat. Mater.* **2**, 408-412 (2003).

40. Choi, J. H. *et al.* Exploiting the colloidal nanocrystal library to construct electronic devices. *Science* **352**, 205-208 (2016).

41. Hunter, R. J. Foundations of Colloid Science. Volume 1 (Oxford University Press Inc., New York, 1986).

42. Li, H., Fauquignon, M., Haddou, M., Schatz, C. & Chapel, J. P. Interfacial Behavior of Solid- and Liquid-like Polyelectrolyte Complexes as a Function of Charge Stoichiometry. *Polymers* **13**, 3848 (2021).

43. Rao, V. & Johns, J. Mechanical properties of thermoplastic elastomeric blends of chitosan and natural rubber latex. *J. Appl. Polym. Sci.* **107**, 2217-2223 (2008).

44. Yuan, J. *et al.* Fabrication and dielectric properties of advanced high permittivity polyaniline/poly(vinylidene fluoride) nanohybrid films with high energy storage density. *J. Mater. Chem.* **20**, 2441-2447 (2010).

45. Yuan, J. *et al.* Giant dielectric permittivity nanocomposites: realizing true potential of pristine carbon nanotubes in polyvinylidene fluoride matrix through an enhanced interfacial interaction. *J. Phys. Chem. C.* **115**, 5515-5521 (2011).

46. Li, W. *et al.* Electric energy storage properties of poly(vinylidene fluoride). *Appl. Phys. Lett.* **96**, 192905 (2010).

47. Fan, B. *et al.* Improving dielectric strength of polyvinylidene fluoride by blending chains with different molecular weights. *Polymer* **190**, 122235 (2020).

48. Torres-Canas, F., Yuan, J., Ly, I., Neri, W., Colin, A., & Poulin, P. Inkjet Printing of Latex-Based High-Energy Microcapacitors. *Adv. Funct. Mater.* **29**, 1901884 (2019).

49. Zheng, M. *et al.* Enhanced breakdown strength of poly(vinylidene fluoride) utilizing rubber nanoparticles for energy storage application. *Appl. Phys. Lett.* **109**, 072902 (2016).

50. Mackey, M. *et al.* Reduction of dielectric hysteresis in multilayered films via nanoconfinement. *Macromolecules* **45**, 1954-1962 (2012).

51. Chen, J. *et al.* Rational design and modification of high-k bis (double-stranded) block copolymer for high electrical energy storage capability. *Chem. Mater.* **30**, 1102-1112 (2018).

52. Li, J. *et al.* Tuning phase transition and ferroelectric properties of poly(vinylidene fluoride-co-trifluoroethylene) via grafting with desired poly(methacrylic ester)s as side chains. *J. Mater. Chem. C.* **1**, 1111-1121 (2013).

53. Guan, F. *et al.* Confinement-induced high-field antiferroelectric-like behavior in a poly (vinylidene fluoride-co-trifluoroethylene-co-chlorotrifluoroethylene)-graft-polystyrene graft copolymer. *Macromolecules* **44**, 2190-2199 (2011).

54. Hougham, G. G., & Jean, Y. C. Relative contributions of polarizability and free volume in reduction of refractive index and dielectric constant with fluorine substitution in polyimides by positron annihilation spectroscopy. *Macromol. Chem. Phys.* **215**, 103-110 (2014).

55. Joyce, D. M. *et al.* Deoxyribonucleic acid-based hybrid thin films for potential application as high energy density capacitors. *J. Appl. Phys.* **115**, 114108 (2014).

56. Gao, Y., Chen, S., Kong, B., Wang, W. & Cheng, Y. IEEE. 866-870. (2020).

57. Zhang, M. *et al.* Controlled functionalization of poly(4-methyl-1-pentene) films for high energy storage applications. *J. Mater. Chem. A.* **4**, 4797-4807 (2016).

58. Treich, G. M. *et al.* Optimization of organotin polymers for dielectric applications. *ACS Appl. Mater. Interfaces.* **8**, 21270-21277 (2016).

59. Che, J. *et al.* Waterborne Nanocomposites with Enhanced Breakdown Strength for High Energy Storage. *ACS Appl. Energy Mater.* **3**, 9107-9116 (2020).

60. Kang, D., Wang, G., Huang, Y., Jiang, P. & Huang, X. Decorating TiO2 Nanowires with BaTiO3 Nanoparticles: A New Approach Leading to Substantially Enhanced Energy Storage Capability of High-k Polymer Nanocomposites. *ACS Appl. Mater. Interfaces.* **10**, 4077-4085 (2018).

Conflict of Interest

The authors declare no competing interests.

TOC Figure